Nanostructured Photothermal Materials for Environmental and Catalytic Applications

Huige Chen [1,2], **Run Shi** [1,*] and **Tierui Zhang** [1,2,*]

1   Key Laboratory of Photochemical Conversion and Optoelectronic Materials, Technical Institute of Physics and Chemistry, Chinese Academy of Sciences, Beijing 100190, China; chenhuige20@mails.ucas.ac.cn
2   Center of Materials Science and Optoelectronics Engineering, University of Chinese Academy of Sciences, Beijing 100049, China
*   Correspondence: shirun@mail.ipc.ac.cn (R.S.); tierui@mail.ipc.ac.cn (T.Z.)

Abstract: Solar energy is a green and sustainable clean energy source. Its rational use can alleviate the energy crisis and environmental pollution. Directly converting solar energy into heat energy is the most efficient method among all solar conversion strategies. Recently, various environmental and energy applications based on nanostructured photothermal materials stimulated the re-examination of the interfacial solar energy conversion process. The design of photothermal nanomaterials is demonstrated to be critical to promote the solar-to-heat energy conversion and the following physical and chemical processes. This review introduces the latest photothermal nanomaterials and their nanostructure modulation strategies for environmental (seawater evaporation) and catalytic (C1 conversion) applications. We present the research progress of photothermal seawater evaporation based on two-dimensional and three-dimensional porous materials. Then, we describe the progress of photothermal catalysis based on layered double hydroxide derived nanostructures, hydroxylated indium oxide nanostructures, and metal plasmonic nanostructures. Finally, we present our insights concerning the future development of this field.

Keywords: photothermal materials; seawater evaporation; photothermal catalysis; layered double hydroxide

1. Introduction

With the ever-growing demand for energy over the last century, there have been alarming and looming threats to humanity caused by the massive consumption of non-renewable energy sources, such as the growing energy crisis and severe environmental pollution [1–3]. It is compelling for humanity to explore an alternative to fossil energy. Among all renewable energy sources (tidal energy, wind energy, geothermal energy, etc.), solar energy is the most appealing owing to its inherent and unique advantages of abundance, global sustainability, as well as accessible and clean nature [4].

The full utilization of solar energy represents a challenging task. According to the extensive research focused on solar energy, there are mainly three types of solar energy utilization strategies: solar-to-thermal, solar-to-electrical, and solar-to-chemical conversions. Solar-to-thermal conversion in the realms of solar heat collection [2,5,6], photothermal seawater evaporation [7,8], and photothermal catalysis [9,10] has been addressed by considerable published research reports in recent years. Solar-to-electrical conversion is principally utilized in solar cells [11,12] and photoelectrical catalysis [13,14], while solar-to-chemical conversion is mostly studied in the following three types of up-hill reactions: photocatalytic water splitting [15,16], photocatalytic CO_2 reduction [17,18], and photocatalytic nitrogen fixation [19].

Photothermal nanomaterials could efficiently convert absorbed sunlight into local heat energy on the surface of materials [20]. Compared to conventional photocatalysts working at room temperature, photothermal catalysts typically have a broader solar spectrum and a

much higher local reaction temperature [21]. Besides, photothermal catalysis demonstrates the undeniable advantages of low cost and cleanliness with solar energy as a cleaner heat source than the fossil energy-driven thermal catalysis [22]. The above promotes the broad application of photothermal nanomaterials in diversified realms, especially in environmental and catalytic applications [23].

With the emergence of photothermal effects as the strong development potential in environmental and energy catalysis, many efforts have been focused on nanostructured photothermal materials. Up to now, nanomaterials focusing on the application of photothermal effects of plasmonic structures [24], photothermal catalytic hydrogenation reactions [25,26], photothermal catalytic CO_2 reduction [21,27,28], and photothermal seawater evaporation [29,30] have been separately reviewed. However, these reviews provide only a one-sided overview of photothermal nanomaterials. A comprehensive summary of nanostructured photothermal materials from the general principle of materials design to state-of-the-art environment and catalytic applications has yet to be undertaken.

In this review, we firstly discuss the forms of solar energy utilization, novel nanostructured photothermal materials, and regulation strategies to efficiently expand the utilization of sunlight. Subsequently, the research significance of photothermal seawater evaporation and the current research status of two-dimensional (2D) and three-dimensional (3D) nanomaterials are presented. Thirdly, the recent advance of photothermal catalysis is reviewed from three aspects: layered double hydroxide (LDH) derived nanostructured materials, hydroxylated indium oxide ($In_2O_{3-x}(OH)_y$) nanostructured materials, and metal plasmonic nanostructured materials. Finally, the conclusion and outlook of this review are proposed.

2. Photothermal Conversion

2.1. Solar Energy Utilization

Solar energy is produced from the fusion of hydrogen inside the sun [31] and has the following advantages: It is universal, harmless, enormous, and long-lasting. The sun provides the energy needed by living creatures on the earth directly or indirectly [32]. For example, plants convert solar energy into chemical energy and store it in their bodies through photosynthesis. Plants and animals buried in the ground can be transformed into fossil energies (coal, oil, natural gas, etc.) through the evolution of long periods of time [33]. Although the energy radiated by the sun into the earth's atmosphere is only one 2.2 billionth of its total radiant energy, it is as high as 173,000 TW, which means that the light energy reaching the earth from the sun in one hour could provide the annual global energy consumption [34]. If solar energy can be efficiently converted and utilized, human society would no longer worry about energy and environmental issues [33,35].

Nowadays, three primary forms of solar energy utilization have been frequently studied. Solar-to-electrical conversion demonstrates its application in the field of solar cells and photoelectric catalysis [11–14]. Solar cells are devices used to directly convert solar energy into electrical energy with the help of the photovoltaic effect [33]. After more than 100 years of development, solar cells have gone through three stages of development. The first generation of solar cells mainly involve monocrystalline silicon and polycrystalline silicon solar cells. The second-generation solar cells are manufactured with various thin-film substrates, mainly CdTe and amorphous silicon thin-film cells [31,32,36]. At present, the third-generation solar cells are in the research and development stage, among which dye-sensitized solar cells, chalcogenide solar cells, and organic solar cells are promising photovoltaic technologies for both outdoor and indoor applications [37–39]. With the growing urgent need to develop sustainable energy sources, photoelectric catalysis is used to convert solar energy into chemical energy for energy production, such as water splitting, CO_2 reduction, and nitrogen fixation [40–42].

Solar-to-chemical conversion is the conversion of light energy into chemical energy by simulating the photosynthesis of plants. Since Fujishima and co-workers used light energy to decompose water on TiO_2 films in 1972 [43], photocatalytic technology has broadened the application areas of photochemical conversion, mainly focusing on up-hill photochemical

synthesis [16–19]. For example, photocatalytic water splitting mainly uses ultraviolet and visible light in the solar spectrum to decompose water into hydrogen and oxygen [16]. Hydrogen has received great attention regarding the high calorific value and environmental friendliness of combustion products. Therefore, hydrogen production from the photolysis of water is considered an ideal strategy for renewable energy production [44]. In the context of the increasing global CO_2 concentration year by year and the environmental problems caused by the greenhouse effect, great effort has also been put into photocatalytic CO_2 reduction for the production of C1 (CO, CH_4, CH_3OH) and C2 (C_2H_5OH) high value-added fuels [17,45,46]. Nitrogen-based compounds have an essential role in the agricultural and chemical industries. The Haber–Bosch process has harsh reaction conditions, requires high temperatures and pressures, consumes a lot of energy, and pollutes the environment [19]. The photocatalytic nitrogen fixation process can reduce N_2 to NH_3 under mild conditions, providing a carbon-free path to safer, cleaner, and sustainable NH_3 production [47].

The third solar energy utilization strategy is solar-to-heat energy conversion and this has been widely investigated in environmental and energy fields, such as photothermal seawater evaporation [48–51] and photothermal catalysis [10,28,52]. In contrast to the former two solar energy utilization strategies, of which the efficiency is restricted by the large bandgap and severe charge recombination of the materials, solar-to-thermal conversion based on the photothermal effect of black nanomaterials can effectively utilize the energy of visible and infrared light by converting low energy photons into local heating. The strategy is demonstrated to help drive multiple physical and chemical processes on the surface of nanostructured photothermal materials and will be discussed in detail in Sections 3 and 4.

2.2. Photothermal Materials and Regulation Strategies

Theoretically, the potential photothermal materials should have the following characteristics: (i) broad spectrum absorption, (ii) high photothermal conversion efficiency, (iii) processability and physicochemical stability, and (iv) low cost. In practical applications, exploring such ideal photothermal materials remains a very challenging issue. Even so, persistent efforts have been devoted to exploring suitable nanomaterials in favor of photothermal conversion, which can be mainly summarized as noble metal materials [53–56], transition metal materials [9,57,58], carbon materials [59,60], and other non-metallic materials [61–63], as shown in Figure 1. Moreover, corresponding modulation strategies have been investigated for different classes of photothermal materials to further boost photothermal efficiency.
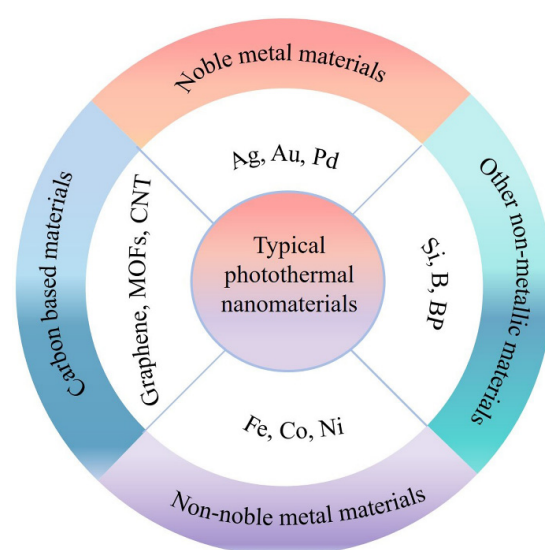

Figure 1. Schematic illustration of typical photothermal nanomaterials.

2.2.1. Metallic Materials

Noble metal materials: The local surface plasmon resonance (LSPR) effect of noble metal nanomaterials (Au [53], Ag [54], Pd [55,64]) has developed them into star materials in photothermal effect researches. The LSPR wavelength of metallic materials can be tuned from ultraviolet (UV) to visible (Vis) and near-infrared (NIR) region, which enables the broad spectral absorption of sunlight and its effective conversion to thermal energy by nonradiative damping [48,65]. There is a tremendous challenge for scientists to seek effective strategies to produce upgraded LSPR light absorption characteristics at specific wavelengths [66]. The first strategy is to tune the absorption wavelength region by adjusting the shapes and sizes of noble metal nanostructures. For example, commonly seen Pd nanostructures (nanocage, nanoplate) only show LSPR peaks in the UV-Vis region. For the first time, Zheng et al. synthesized Pd nanosheets with a thickness of less than ten atomic layers by fine-tuning the Pd nanostructure. They found that the ultrathin structure enabled it to have LSPR absorption in the NIR region and convert the absorbed light into heat, which was the main reason for the superior catalytic performance exhibited by Pd nanosheets compared with commercial palladium black [55]. The plasmonic coupling effect of forming hot-spot regions between two metal nanoparticles is the second way to adjust the light absorption property of noble metal nanostructures. For example, the plasmonic coupling effect of Pt and Au on Pt-Au/SiO_2 material endowed the catalysts to efficiently utilize UV-Vis light energy, generating more hot electrons, thus reducing the activation energy of CO_2 molecules [67]. The third strategy is to control the interaction between the metal and the support to modulate the structure of the absorption center. The Pd/ZnO catalyst reported by Hong's group displayed a weak and broad light absorption with its LSPR redshift to near 570 nm, which might be related to the formation of PdZn alloys due to the strong-metal-support-interaction [64].

Non-noble metal materials: Due to the high cost and low earth content of noble metals, non-precious transition metals have recently gained interest in many catalytic reactions. Among the transition metal family, Fe-based, Co-based, and Ni-based nanostructures with CO_2 hydrogenation activity, Fischer–Tropsch synthesis (FTs) activity, reverse water gas shift (RWGS) activity, and dry reforming of methane (DRM) activity are breaking star materials in the field of photothermal catalysis. The Fe-based catalysts with RWGS and FTs activities are mostly used in CO_2 hydrogenation reaction studies, which generate high-value hydrocarbons (C_{2+}) [68–70]. However, the selectivity of the Fe-based catalysts for C_{2+} products is not very satisfactory. To this end, Zhang's team used a strategy of combining Fe with Co, which shows high C-C coupling ability in FTs, to synthesize CoFe nanoalloys, achieving high C_{2+} selectivity (35.26%) [57]. Recently, the team developed a low-cost Fe-containing catalyst via the hydrogen reduction of MgFeAl-LDH nanosheets [9]. The as-prepared photothermal catalyst composed of Fe and FeO_x showed further enhanced C_{2+} selectivity (52.9%). The heterogeneous structure composed of partially oxidized metallic Fe nanoparticles played an important role in improving the C-C coupling kinetics to suppress methane formation. Co-based catalysts are the preferred catalysts for FTs, with the advantages of (i) abundant reserves, (ii) good resistance to sintering, (iii) high selectivity to long-chain liquid hydrocarbons [71]. In the past years, researchers have devoted themselves to studying Co-based catalysts in generating fuels and olefins from FTs. Doping or modification of Co with nonmetallic elements (C or N) is a strategy to adjust the charge density of Co-based nanomaterials and contribute to enhanced photothermal performances. For example, cobalt nanocrystals modified with C with excellent light olefins ($C_{2-4}{}^=$) selectivity were reported by Sun et al. [72]. Compared with Fe-based and Co-based catalysts, Ni-based catalysts have relatively high DRM activity and good stability. However, under light irradiation-induced high-temperature reaction conditions, Ni-based catalysts are prone to carbon accumulation on the surface, which is detrimental to the reaction process. Li's team designed a novel catalyst system by loading SiO_2 clusters modified with Ni-temporal nanocrystals on mesoporous SiO_2 to effectively suppress the carbon build-up during the reaction, thus improving the activity and stability of the catalyst [58].

2.2.2. Metal-Free Materials

Carbon materials: In contrast to metallic materials, carbon materials (graphene materials [73], carbon-based single atom materials [60], metal-organic-framework derivates [74], and carbon nanotube materials [75]) have come to represent one of the ideal photothermal materials due to their high specific surface area, good thermal conductivity, broad spectral absorption, and low cost. The strong light absorption ability and high thermal conductivity of graphene are gaining increasing interest for photothermal applications. Recently, several works have reported that the coupling effect of transition metals with carbon materials can enhance photothermal performance [76,77]. For instance, Pd single atom-loaded nitrogen-doped graphene had been synthesized, achieving excellent acetylene selective hydrogenation performance with high acetylene conversion (99%), ethylene selectivity (93.5%), and good photostability [60]. The modification of the topological structure of carbon materials can also enhance the photothermal conversion efficiency. Liu et al. synthesized black monodisperse mesoporous carbon nanospheres with a specific surface area of about 950 m^2 g^{-1} by carbonization of ZIF-8 organometallic framework [74]. The material exhibited excellent photothermal conversion efficiency (33.0%) and outstanding photostability than commonly used photothermal agents (Au, Bi_2S_3, $Cu_{2-x}S$) under 808 nm NIR light irradiation. Besides, the construction of the 3D porous structure of carbon materials can increase the light-harvesting capacity to enhance the solar-to-thermal conversion efficiency, such as 3D porous g-C_3N_4/GO aerogel [59].

Other metal-free materials: In addition to carbon-based photothermal materials, other non-metallic materials, such as silicon [63,78], boron [62], and black phosphorus [79], have also attracted a lot of attention in photothermal catalysis. Silicon is an earth-abundant non-metallic element and has been well developed in the industry. Ozin's team used silicon nanowires (Si NWs) as support to load with non-stoichiometric hydroxylated $In_2O_{3-x}(OH)_y$ and ruthenium nanoparticles, respectively, and showed that the presence of Si NWs could significantly improve the light-harvesting ability of the composite catalysts and further enhance the reaction rate [63,78]. Boron has demonstrated unique superiority in solar light absorption and photothermal conversion due to its unique band structure. For example, Ye et al. reported for the first time that the strong absorption of boron catalysts in the UV-Vis and even NIR regions, which contributed to the excellent local photothermal effect to directly reduce CO_2 to CO and CH_4 [62]. In addition, black phosphorus (BP) with a graphene-like layered structure possesses a broad spectrum of absorption to NIR and is often combined with other materials in certain ways to achieve enhanced light absorption, which is mainly used in photothermal therapy [61]. Liu's team reported BP-based nanocomposites as NIR-responsive nano-agent-triggered photothermal materials for high-performance cancer photoimmunotherapy [79].

Generally, both physical evaporation and chemical reaction are temperature-correlated processes, of which the efficiency is highly dependent on the local temperature of the microenvironment. The nanostructured photothermal materials discussed above have been intensively investigated in the fields of seawater evaporation-related environmental applications and clean energy catalysis in recent years, and we summarize the structure–property relationship during the processes in the following sections.

3. Photothermal Seawater Evaporation

3.1. Research Significance and Status

Freshwater resources face severe shortages as the population grows exponentially and water pollution problems worsen. Currently, nearly one-third of the world's population lacks access to clean water, and it is expected that two-thirds of the world's population will be in water stress by 2025 [80]. Water scarcity is pushing humanity to seek an attractive solution. The use of solar energy for photothermal seawater evaporation has turned out to be a promising approach to the shortage of water resources [48]. Photothermal seawater evaporation technology can obtain drinkable water from seawater and wastewater with the advantages of eco-friendliness and high freshwater purity [81]. Photothermal seawater

evaporation can convert solar energy into local thermal energy on the material surface, providing the required energy for water evaporation. Moreover, people can ulteriorly promote the water evaporation process by increasing the surface temperature and the gas–liquid interface area through photothermal nanostructure modulation. So far, photothermal water evaporation generally has the following three research directions: (i) desalination of seawater, (ii) purification of wastewater, (iii) photothermal steam sterilization [48]. Seawater desalination, as the name implies, is the process of converting seawater into freshwater, using sustainable and non-polluting solar energy to achieve an energy-saving generation of freshwater. Wastewater purification uses photothermal evaporation technology to treat pollutants (e.g., heavy metal ions, phosphates, nitrates, organic dyes, volatile organic compounds, and even coliform bacteria) and achieve environmental remediation while collecting clean water from wastewater. Steam sterilization is a widely used sterilization method. The high-temperature steam generated by photothermal seawater evaporation can play a key role in killing various bacteria. Importantly, efficient evaporation of seawater is inextricably linked to the excellent performance of photothermal materials. In recent years, progress has been made in designing photothermal conversion materials for efficient seawater evaporation. The structure of nanomaterials with excellent photothermal properties can be divided into 2D layered nanostructures and 3D porous nanostructures. Some recent literature on the 2D and 3D nanostructured materials for photothermal seawater evaporation is shown in Table 1.

Table 1. Summary of the research on the 2D and 3D nanostructured materials for photothermal seawater evaporation.

Types of Nanostructures	Photothermal Materials	Solar Illumination (kW m^{-2})	Evaporation Rate/Efficiency	Reference
2D nanostructure	Ti$_3$C$_2$/PVDF membrane	1	84%	[82]
	MoS$_2$ nanosheets	0.76	76%	[83]
	BiInSe$_3$@CF	1	1.1 kg m^{-2} h^{-1}	[84]
	SWNT$-$MoS$_2$ film	5	6.6 kg m^{-2} h^{-1}	[85]
	MoOx HNS	1	1.05 kg m^{-2} h^{-1}	[49]
	Ti$_3$C$_2$T$_x$/cellulose membrane	1	1.44 kg m^{-2} h^{-1}	[51]
	biomimetic Mxene	1	1.33 kg m^{-2} h^{-1}	[86]
	2D defective WOx nanosheets	1	78.6%	[87]
	boron nanosheets modified with MoS$_2$	1	1.538 kg m^{-2} h^{-1}	[88]
	SWNT/AuNR Janus film	5	94%	[89]
	Au/Ti$_3$C$_2$ membrane	2	2.66 kg m^{-2} h^{-1}	[90]
3D nanostructure	cellular nitrogen-enriched CS	1	1.31 kg m^{-2} h^{-1}	[91]
	3D graphene foam	1	2.40 kg m^{-2} h^{-1}	[92]
	modified graphene aerogel	1	76.9%	[93]
	graphite-modified sponge	1	73.3%	[94]
	RGO$-$SA$-$CNT aerogel	1	1.622 kg m^{-2} h^{-1}	[95]
	hollow carbon nanotubes aerogels	1	86.8%	[96]
	Co$-$CNS/MXenes foam	1	93.39%	[97]
	Cu$_3$BiS$_3$/MXenes	1	1.32 kg m^{-2} h^{-1}	[98]
	photo-thermal fiber felt	1	1.48 kg m^{-2} h^{-1}	[99]
	cellulose/alginate/carbon black hydrogel	1	1.33 kg m^{-2} h^{-1}	[100]
	RGO$-$SA$-$cellulose aerogel	1	2.25 kg m^{-2} h^{-1}	[101]

3.2. Two-Dimensional Nanostructures

It is well known that the discovery of graphene has brought 2D nanomaterials into the limelight and inspired researchers to explore their properties and applications [102,103]. Recent studies have shown the unique properties of 2D materials, such as ultrathin anisotropy structure, high specific surface area, and tunable optical properties, making them stand out in the field of photothermal seawater evaporation [50]. Up till now, transition metal dichalcogenides (TMDs) [85], transition metal oxides (TMOs) [49], MXenes [51], and other

materials in the family of 2D materials have been reported in photothermal seawater evaporation. For example, the strong light absorption and LSPR properties endow TMOs with a high photothermal conversion capacity [50]. Wang et al. reported an atomic-scale thickness of oxygen-defected molybdenum oxides hierarchical nanostructure (MoO$_x$ HNS) photothermal nanomaterial for seawater evaporation [49]. The water evaporation rate of the MoO$_x$ HNS membrane was 1.255 kg m^{-2} h^{-1} under one sun irradiation, achieving a high energy conversion efficiency of 85.6% (Figure 2a,b). Furthermore, MoO$_x$ HNS with oxygen vacancies and unique flower-like nanoplate structures exhibited broad-spectrum absorption properties (from Vis to NIR light) (Figure 2c), which might be attributed to the electron leap between the valence band, defective energy levels, and conduction band (Figure 2d,e). This study provides a new idea for the future industrial preparation of high-performance and low-cost photothermal seawater evaporation materials.
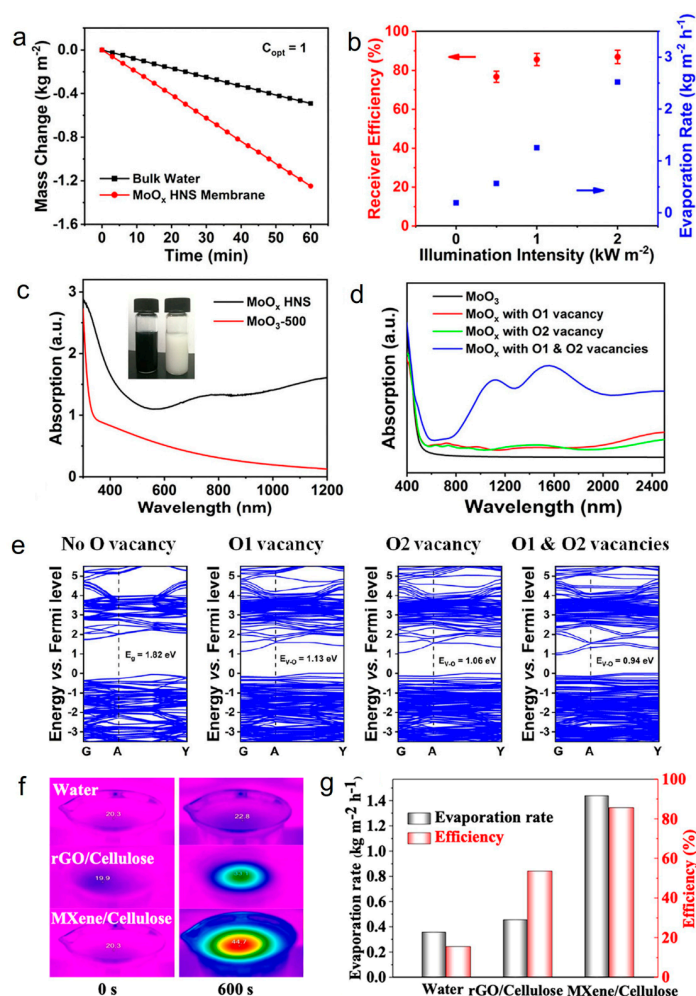

Figure 2. (**a**) Mass change of bulk water and water covered with different MoO$_x$ HNS membranes under one sun. (**b**) The evaporation rate and corresponding receiver efficiency of the MoO$_x$ HNS membrane under different illumination intensities. (**c**) UV−Vis−NIR absorption spectra of the MoOx HNS and MoO$_3$−500 (The MoO$_3$ sample was treated via air-oxidation at 500 °C). Inset: optical photos of MoOx HNS (left) and MoO$_3$−500 (right) aqueous solutions. (**d**) Simulated optical absorption spectra. (**e**) Simulated band structures of the molybdenum oxides with different concentrations of oxygen vacancies. Reprinted with permission from ref. [49]. Copyright 2019 Wiley-VCH. (**f**) IR thermal images of bulk water, MXene/cellulose, and rGO/cellulose membrane surface. (**g**) Water evaporation rates and solar steam efficiency of bulk water, rGO/cellulose, and MXene/cellulose membranes under the solar illumination of 1 sun. Reprinted with permission from ref. [51]. Copyright 2019 American Chemical Society.

MXenes is a class of materials consisting of a few atomic layers of transition metal carbides, nitrides, or carbonitrides that has been investigated a lot for photothermal seawater evaporation due to its excellent hydrophilicity, large specific surface area, and electromagnetic wave absorption, which lead to outstanding photothermal conversion properties [104,105]. For instance, Yang's team synthesized $Ti_3C_2T_x$/cellulose membrane through the dip-coating method where $Ti_3C_2T_x$ was coated on cellulose membrane and explored the photothermal seawater evaporation properties of the material [51]. MXenes/cellulose membranes exhibited surprising light absorption efficiency (94%) in the 300–1500 nm spectral range and a higher photothermal conversion efficiency than volumetric water and rGO/cellulose membranes (Figure 2f). It is noteworthy that the MXenes/cellulose membrane achieved an evaporation efficiency of up to 85.6% under one sun irradiation (Figure 2g). In addition, the MXenes/cellulose membranes exhibited good stability under ultrasonic treatment and strong mechanical agitation. In short, the strong light absorption, high photothermal conversion efficiency, good stability, and excellent evaporation efficiency of MXenes/cellulose membranes made it possible to use sunlight for seawater evaporation to obtain clean water in a long-term and sustainable way.

3.3. Three-Dimensional Porous Nanostructures

Although 2D structured nanomaterials show some superiority in photothermal seawater evaporation, as described in Section 3.2 above, such materials still have shortcomings limiting the further improvement of photothermal performance. On the one hand, 2D materials are prone to refraction at the solid–liquid interface due to the Fresnel effect and thus lose light at specific wavelengths [106]. On the other hand, 2D materials have low light reflectivity due to their planar structure, which often leads to poor repeated utilization of light [107]. Hence, 3D porous nanostructures materials such as sponge-like materials [91,92] and aerogels [93] are ideal materials for photothermal seawater evaporation materials due to their pore structure, porosity, and richness of pores, where light can be reflected and scattered multiple times and enhance the light-material interaction, which is an improvement in addressing the shortcomings of 2D materials. Taking carbon sponge (CS) as an example, Ho et al. used a scalable 3D elastic nitrogen-rich porous CS for efficient in situ indirect photothermal evaporation [91]. The CS was floated at the water–air interface so that the photothermal effect of CS heated the interfacial water under light irradiation, and the CS with a minimum pore size of 25 μm (CS25) showed the best photothermal evaporation rate (1.31 kg m^{-2} h^{-1}) after one hour of stable evaporation (Figure 3a) The surface temperature of the CS reached approximately 47 °C (Figure 3b). In addition, the CS exhibited a stable photothermal performance in the cycling test with no significant performance decline (Figure 3c). The broadband optical absorption and the embedded elastic porous pore structure contributed to CS's ability to avoid excessive heat loss and improve evaporation efficiency. In addition, Wang's team prepared hydrophilic reduced graphene oxide aerogel (MGA) with photothermal seawater evaporation efficiency of 76.9% under one sun irradiation (Figure 3d) [93]. The hydrophilic 3D network nanostructure of MGA increased the local temperature under irradiation and allowed efficient interfacial water transportation to the photothermal surface, thus contributing to an enhanced evaporation efficiency.
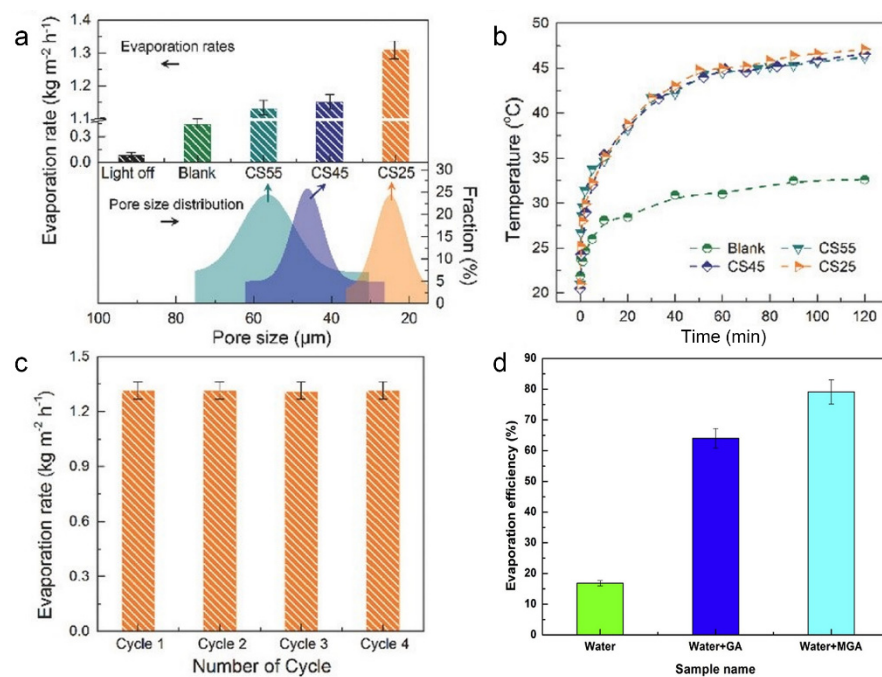
Figure 3. The evaporation rates (**a**) and surface temperature changes (**b**) of different CS at an optical density of 1 kW m^{-2}. (**c**) Stability and reusability of CS25 for steam generation. Reprinted with permission from ref. [91]. Copyright 2018 Wiley-VCH. (**d**) The evaporation efficiency of different samples under 1 kW m^{-2} solar irradiation. Reprinted with permission from ref. [93]. Copyright 2018 Elsevier.

4. Photothermal Catalysis

4.1. Reaction Types

In addition to the photothermal seawater evaporation described in Section 3, investigations on solar-to-thermal conversion have been extended to the field of photothermal catalysis with the following main applications: decomposition of organic matter [108], hydrogen production [109,110], CO_2 reduction [111], and CO reduction [52]. Many works have focused on the photothermal catalytic conversion of C1 (CO, CO_2, and CH_4) molecules into valuable chemicals and fuels. Specifically, photothermal C1 catalysis is mainly based on the photothermal effect from visible and infrared irradiation to increase the local temperature of the catalyst to overcome the reaction barriers. Photoexcitation under UV irradiation also plays an important role in optimizing product selectivity by modulating the reaction path of reaction intermediates. Various types of reactions have been developed to explore photothermal C1 catalysis. These reactions will be described as follows.

Photothermal catalytic CO_2 reduction: (i) Methanation of CO_2 ($CO_2 + 4H_2 \rightarrow CH_4 + 2H_2O$) [78,112]. CO_2 reacts with H_2 to form CH_4, known as the Sabatier reaction, which is an exothermic reaction. This reaction is promising in energy conversion, especially in the Power to Gas projects. The promising active catalysts for this reaction are usually group VIII metals or metal oxides [28,111]. (ii) RWGS reaction ($CO_2 + H_2 \rightarrow CO + H_2O$) [112]. CO_2 reacts with H_2 to form CO and H_2O. This reaction can effectively convert CO_2 to CO and is an important way to synthesize high value-added hydrocarbons. $In_2O_{3-x}(OH)_y$ and plasmonic metal nanoparticles (Au, Ru, Al, etc.) are often used to study RWGS reactions owing to their unique photothermal and CO_2/H_2 activation properties that allow them to exhibit superior catalytic activities compared to other catalysts [28]. (iii) CO_2 hydrogenation to C_{2+} hydrocarbon reaction. These reactions produce C_{2+} products such as high carbon alkanes (ethane, propane, etc.) by controlling the hydrogenation capacity of CO_2, which is a promising method for generating high value-added products [28]. (iv) Methanol synthesis ($CO_2 + 3H_2 \rightarrow CH_3OH + H_2O$) [113]. At present, methanol is generated from syngas at high pressures and temperatures in

the industry, which has a large carbon footprint. CO_2 has been gradually used to replace CO and react with H_2 for sustainable methanol production. Recently, $In_2O_{3-x}(OH)_y$ nanocrystal superstructure [114], Cu/ZnO [115], Na-Co@C [116], Au&Pt@ZIF [117] have been used to study photothermal methanol formation [111]. (v) Dry reforming reaction $(CO_2 + CH_4 \rightarrow 2H_2 + 2CO)$ [118,119]. This reaction converts two major greenhouse gases (CO_2 and CH_4) into syngas and subsequently produces clean energy through FTs. Group VIII metals (Rh, Pd, Pt, Ni, Co) have shown good photothermal activity for the DRM reaction [111].

Photothermal catalytic CO conversion: (i) Fischer–Tropsch synthesis. The FTs reaction is a catalytic reaction in which synthesis gas is used as the initial feedstock to produce long-chain alkanes, olefins, and higher alcohols under high temperatures and pressures in the presence of certain catalysts. Over the years, Ni-based, Co-based, Fe-based, and Ru-based catalysts have been extensively studied for FTs [120–123]. (ii) Water-gas shift (WGS) reaction $(CO + H_2O \rightarrow CO_2 + H_2)$ [124]. The WGS reaction, which is the reaction of CO and H_2O to form H_2 and CO_2, is gaining attention as a side reaction in the FTs reaction and is widely used in industrial hydrogen production and CO removal as an exothermic reaction [111]. Metal-loaded catalysts (e.g., CuO_x/Al_2O_3) are mostly used to study the WGS reaction [125].

4.2. LDH Topological Transformation Nanostructures

LDH is composed of positively charged laminates, interlayer anions, and water molecules, showing a similar structure to hydromagnesite $Mg(OH)_2$, and the main laminate is formed by the shared prism of NO_6 octahedra [126]. The general formula of LDH material is $[M_{1-x}^{2+}M_x^{3+}(OH)_2]^{q+}A_{x/n}^{n-}\cdot\gamma H_2O$, where M^{2+} and M^{3+} represent divalent and trivalent cations, respectively, and A is the interlayer anion. In general, the common divalent cations forming LDH are Mg^{2+}, Ni^{2+}, Zn^{2+}, Co^{2+}, Fe^{2+}, Mn^{2+}, Ca^{2+}, and Cu^{2+}, and common trivalent cations are Cr^{3+}, Fe^{3+} and Al^{3+} [127]. The intercalated anions between the LDH layers can be chosen from I^-, F^-, Cl^-, Br^-, OH^-, CO_3^{2-}, SO_4^{2-}, and PO_4^{3-} [128].

The outstanding features of variable chemical composition and tunable morphology mean LDH often serve as an effective precursor for highly dispersed metal-loaded catalysts [129]. In recent years, LDH-based photothermal catalysis is mainly focused on CO and CO_2 hydrogenation [52,121]. Recent literature on the LDH-derived materials for photothermal C1 conversion is summarized in Table 2. For example, Zhang et al. obtained a series of Co-based catalysts with different phase compositions by the thermal reduction of ZnCoAl-LDH with H_2 at different temperatures (from 300 to 700 °C) [121] Among them, the Co_3O_4/Co nanocatalysts obtained by the reduction at 450 °C achieved up to 36% selectivity of $C_{2-4}{}^=$ olefins under the light condition. The structural characterization confirmed that the interfacial structure composed of nano-scale Co_3O_4 and monomeric Co was the active phase of the reaction. Further, theoretical calculations showed that the Co_3O_4/Co interfacial structure weakened the over-hydrogenation ability of metallic Co, thus increasing the selectivity of low-carbon olefins.

Table 2. Summary of the research on the LDH-derived materials for photothermal CO/CO_2 conversion.

Reaction Type	Catalyst	Reaction Temperature (°C)	Rate/Selectivity			Reference
			CO	CH$_4$	C$_{2+}$	
CO conversion	Fe−500	230	-	28.6%	60%	[122]
	Co−700	210	-	35%	65%	[52]
	Co−450	195	-	48%	52%	[121]
CO$_2$ conversion	CoFe-650	310	4.97%	59.77%	35.26%	[57]
	Ru@FL-LDHs	350	-	277 mmol g^{-1} h^{-1}	-	[130]
	Fe−500	275	-	47.1%	52.9%	[9]
	Ni−600	290	-	278.8 mmol g^{-1} h^{-1}	-	[131]

In a subsequent study, Zhang et al. obtained a series of Co-based catalysts with different phase compositions by reducing CoAl-LDH nanosheets in a hydrogen atmosphere under different temperatures (Co_3O_4 for temperature below 600 °C and Co(0) for temperature above 600 °C) [52]. Among them, the Co-700 catalysts obtained by reduction at 700 °C achieved up to 65% C_{2+} selectivity (~36.3% C_{2-4} and ~28.7% C_{5+}) under UV-Vis irradiation. Density functional theory (DFT) calculations confirmed that the high selectivity for high hydrocarbons was due to the formation of metallic Co nanoparticles that enhance the C-C coupling ability of LDH-derived catalysts (Figure 4a,b). In addition to FTs, photothermal CO_2 hydrogenation based on LDH nanostructures has also been investigated. Ye et al. reported the photothermal CO_2 hydrogenation to CH_4 based on Ru-loaded ultrathin MgAl-LDH in a gas-flowing reactor, achieved a high CH_4 production rate of 277 µmol g^{-1} h^{-1} owing to the abundant surface OH groups of LDH to facilitate the chemosorption and activation of CO_2 molecules [130]. Besides, it was found that the Fe-based nanocatalysts composed of Fe and FeO_x formed by reducing precursors at 500 °C had high C_{2+} selectivity (52.9%) for CO_2 hydrogenation under UV-Vis light irradiation [9]. The results showed that Fe(0) and FeO_x were the active phases of Fe-500 catalysts and that the Fe(0)/FeO_x ratio was optimal at this point, with excess Fe(0) leading to high CH_4 selectivity. The significant role of FeO_x in modulating the electronic structure of metallic Fe nanoparticles inhibited CH_2 and CH_3 over-hydrogenation on Fe(0) nanoparticles, thereby enhancing the C-C coupling reaction (Figure 4c,d). In conclusion, the heterogeneous structure consisting of partially oxidized metal Fe nanoparticles was the main factor that improved the photothermal catalytic FTs selectivity towards C_{2+} products.
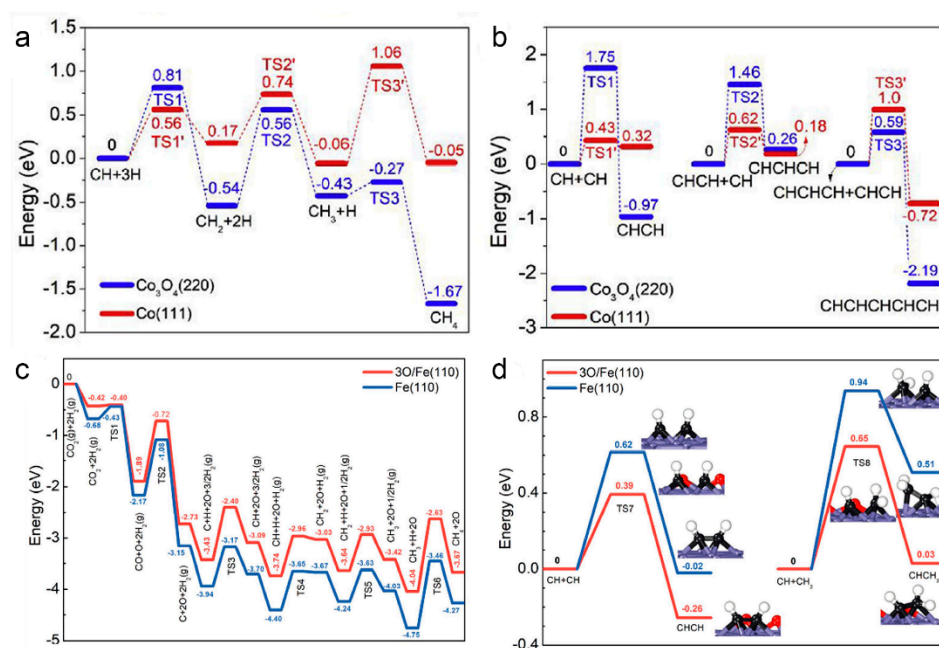

Figure 4. The potential energy profile of (**a**) CH_4 formation and (**b**) C−C coupling on Co_3O_4 (220) and Co (111). Reprinted with permission from ref. [52]. Copyright 2019 Elsevier. The potential-energy profiled of the possible pathways for CO_2 conversion on 3O/Fe (110) and Fe (110). (**c**) CH_4 formation and (**d**) C−C coupling reactions. The insets in (**d**) show the configurations of the transition and final states of C−C coupling. The blue, black, red, and white spheres represent Fe, C, O, and H atoms, respectively. Reprinted with permission from ref. [9]. Copyright 2021 Wiley-VCH.

4.3. $In_2O_{3-x}(OH)_y$ Nanostructures

$In_2O_{3-x}(OH)_y$ has received great attention as a promising photothermal material due to its unique surface, optical, and electronic properties. Its surface is rich in active sites (oxygen vacancies and hydroxide defects), where the hydroxide defects can efficiently adsorb CO_2 and enhance the ability of CO_2 capture and activation in RWGS reaction [132].

In recent years, many efforts have been made to study RWGS performance over $In_2O_{3-x}(OH)_y$ and explore strategies to improve RWGS performance by Ozin's group [133,134]. Ozin and co-workers investigated for the first time the effect of oxygen vacancies and hydroxide defects on $In_2O_{3-x}(OH)_y$ for the RWGS reaction employing the combination of spectroscopic, kinetics, and DFT calculation [133]. They examined the performance of the photothermal RWGS in a flow reactor, and the rate for CO production was 4-fold higher under light irradiation (153 μmol g^{-1} h^{-1}) than under dark conditions (35.7 μmol g^{-1} h^{-1}) at the same temperature (190 °C). The results of this study revealed that the Lewis basic hydroxyl radicals and Lewis acidic indium atoms located near the oxygen vacancies worked synergistically to dissociate H_2 and activate CO_2, which subsequently generated CO and H_2O (Figure 5a). In addition, the increase in RWGS reaction activity could be attributed to the decrease in activation energy due to Lewis alkalinity and Lewis acidity of the excited state enhanced by photoexcited electrons/holes trapped at the frustrated Lewis pairs (FLPs) site. In the following study, in order to reduce the cost of using $In_2O_{3-x}(OH)_y$ while ensuring sufficient active site exposure, Ozin's group also synthesized a series of ternary heterostructured catalysts ($ntTiN@ncTiO_2@ncIn_2O_{3-x}(OH)_y$) via an electrochemical method, where one-dimensional TiN nanotube periodic arrays, TiO_2 and $In_2O_{3-x}(OH)_y$ were sequentially arranged from the inside to the outside (Figure 5b) [134]. The $ntTiN@ncTiO_2@ncIn_2O_{3-x}(OH)_y$ catalyst exhibited an incredible RWGS activity of 81.1 mmol g^{-1} h^{-1} (Figure 5c). The analysis of the experimental results indicated that the enhancement of catalytic activity was due to the combination of the following three factors: (i) the defective RWGS active sites on the surface of $In_2O_{3-x}(OH)_y$ located in the ternary catalyst (ii) the photothermal effect of TiN that provided a photothermal driving force for the reaction, and (iii) the electron transfer between TiO_2 and $In_2O_{3-x}(OH)_y$ that enhanced the CO_2 hydrogenation ability (Figure 5d).

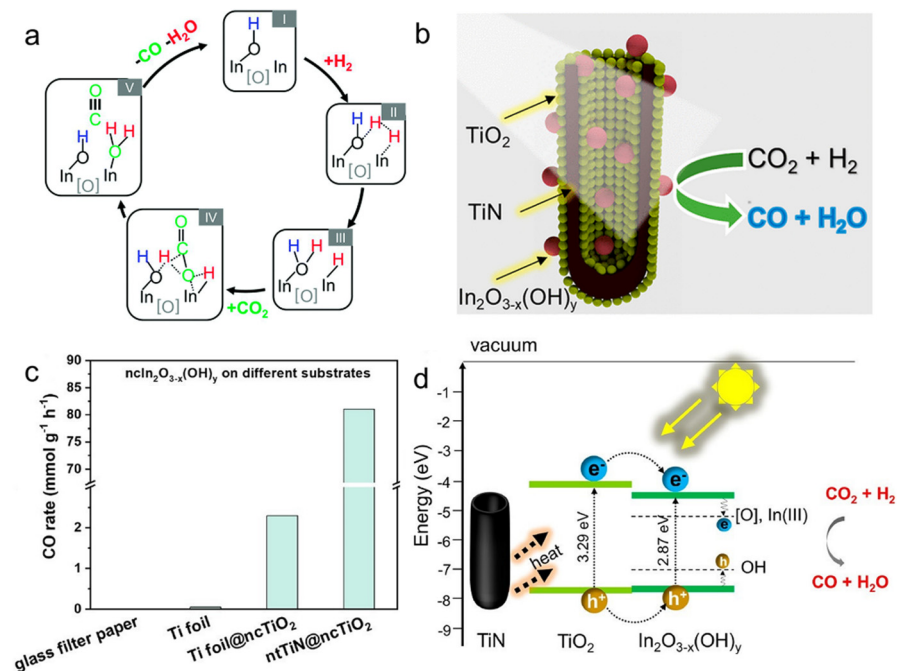**Figure 5.** (**a**) Overall proposed mechanism for the RWGS reaction on $In_2O_{3-x}(OH)_y$. Reprinted with permission from ref. [133]. Copyright 2015 Royal Society of Chemistry. (**b**) The schematic diagram of $ntTiN@ncTiO_2@ncIn_2O_{3-x}(OH)_y$. (**c**) nc $In_2O_{3-x}(OH)_y$ supported on different substrates (borosilicate glass microfiber filter paper, Ti foil, Ti foil decorated with $ncTiO_2$, and ntTiN decorated with $ncTiO_2$). (**d**) Proposed activation mechanism for the photocatalytic reaction. Reprinted with permission from ref. [134]. Copyright 2021 American Chemical Society.

Recently, $In_2O_{3-x}(OH)_y$ has also been used to study the activity of photothermal CO_2 hydrogenation to methanol [114]. $In_2O_{3-x}(OH)_y$ nanocrystal superstructures with 161.21 m^2 g^{-1} specific surface area and 3–7 nm pore size distribution for methanol generation reaction were synthesized by Ozin et al. They explored the effects of different temperatures (200 °C, 250 °C, 300 °C) on the products at atmospheric pressure in a flow reactor. The optimal temperature for the photothermal synthesis of methanol was 250 °C, which reached the highest methanol yield (97.3 µmol g^{-1} h^{-1}) with more than 50% selectivity under light illumination. The main reasons for the high methanol yield were the superstructure of $In_2O_{3-x}(OH)_y$ and the unique conformation of the FLPs sites on the surface.

4.4. Metal Plasmonic Nanostructures

As discussed in Section 2.2.1, plasmonic nanometals can effectively convert incident UV, visible, and even NIR photons into heat energy through an LSPR mechanism, providing a direct, fast, energy-efficient, and targeted heating method for local reaction sites where catalytic reactions occur [10]. Group VIII nanometals may be the most promising candidate for plasmonic photothermal catalysis.

The light absorption of group VIII plasmonic nanometals covers almost the entire solar spectrum, making them be ideal catalysts for photothermal DRM [28,135,136]. Ye et al. synthesized Pt/TaN catalyst by impregnation method and investigated its catalytic activity with DRM as the reaction [135]. The experimental results showed that the Pt/TaN catalyst had excellent photothermal DRM activity, and the selectivity of the products CO and H_2 was close to 100% (Figure 6a). In addition, the rate of activity enhancement of Pt/TaN activity was very significant compared with the introduction of Au into Pt/Ta_2O_5, which indicated that TaN was an attractive optical body to improve the activity of the loaded catalyst. The reason for the enhanced activity of Pt/TaN catalyst was mainly related to the polar electrostatic field on the surface of TaN. Specifically, as shown in Figure 6b,c, electrons and holes were not easily recombined under the build-in electric field induced by the polarity of TaN. Subsequently, electrons reduced the adsorbed CO_2 to CO, and holes oxidized CH_4 for H_2 evolution, contributing to an outstanding DRM activity. Besides, Ye's group explored the effect of different particle sizes of nickel loaded on Al_2O_3 on the DRM reaction and found that different particle size ranges led to different photothermal activities [136]. Among them, 10 wt.% Ni loading onto Al_2O_3 (10 Ni/Al_2O_3) catalyst obtained the highest catalytic performance. Under 400–500 nm irradiation, the activity of 10 Ni/Al_2O_3 was increased by 1.3 times compared to the catalyst in the dark condition, even at a low light intensity of 0.06 W cm^{-2}. The LSPR effect was demonstrated to be the main reason for the improved photothermal activity when the size of nickel was less than 17.2 nm, while an interband jumping mechanism on the nickel particles was the dominant reason when the size of a nickel particle was larger than 33.5 nm.

Besides, iron@carbon core-shell nanoparticles with surface-enhanced LSPR effect were obtained owing to the plasmonic coupling between metal core and thin carbon layers [137]. The temperature of the core-shell nanostructure reached 481 °C under irradiation, achieving an RWGS reaction CO yield of 2196 µmol for 120 min. Ye's team also investigated the steam methane reforming (SMR) activity of Rh [138]. They used an impregnation method to load precious metal Rh nanoparticles on TiO_2. Under visible light conditions (580 mW cm^{-2}), the Rh/TiO_2 catalyst converted CH_4 to H_2. With a 50% reduced activation energy compared to catalysis in the absence of light. Experimental characterization and theoretical calculations showed that the hot carriers at the interface between Rh and TiO_2 could quickly separate, leading to the formation of electron-deficient $Rh^{\delta+}$ on their surfaces, thus activating the carbon-hydrogen bond and enabling the further activation of methane at low temperatures (Figure 6d).
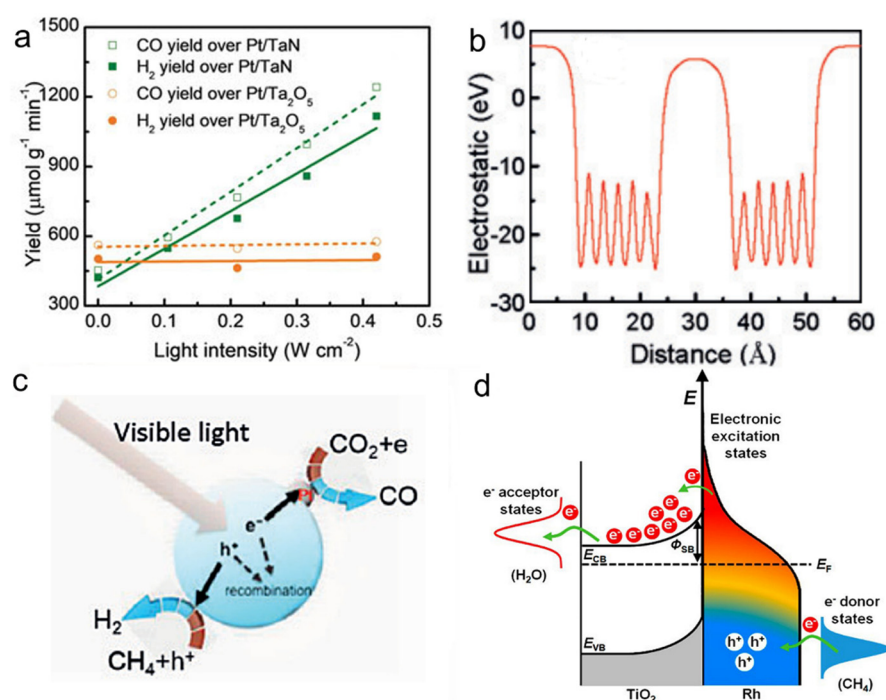
Figure 6. (**a**) Catalytic performance of Pt/TaN and Pt/Ta$_2$O$_5$ for DRM reaction to produce CO and H$_2$. (**b**) The distribution of the electrostatic field over TaN, and (**c**) Proposed mechanism of the DRM reaction over Pt/TaN catalyst under visible light irradiation. Reprinted with permission from ref. [135]. Copyright 2018 Wiley-VCH. (**d**) Schematic of energy transfer from photoexcited hot carriers to adsorbate states and proposed mechanism for SMR reaction on Rh/TiO$_2$ under illumination. Reprinted with permission from ref. [138]. Copyright 2018 American Chemical Society.

5. Conclusions and Future Outlook

In this review, we firstly discussed a series of important photothermal nanomaterials (noble metals, transition metals, carbon-based materials, etc.) and proposed the corresponding materials' modulation strategies to enhance the photothermal performance, and briefly outlined the recent progress of photothermal nanomaterials in the field of photothermal seawater evaporation and photothermal catalysis. Among them, photothermal seawater evaporation was mainly described in terms of the structure of materials (2D structures, 3D structures), while the consideration photothermal catalysis focused on the active site modification over typical photothermal catalytic nanomaterials, summarized the advantages of these materials, and discussed different types of photothermal catalytic reactions. Although research progress has made for photothermal nanomaterials for environmental and energy applications, shortcomings still need to be further addressed.

Firstly, the application of the photothermal effect in non-gas-solid phase catalytic reaction systems (such as liquid-solid phase, gas-solid-liquid triplet phase) has not been thoroughly investigated. Secondly, the application of new photothermal nanomaterials in more energy and environmental processes needs to be further developed. At present, the application of photothermal materials in the environment has only been demonstrated in the field of seawater evaporation. Therefore, future research should focus on combining photothermal catalysis with environmental treatment, such as the photothermal catalytic degradation of pollutants and degradation and conversion of plastics.

In addition to the above mentioned, there are still some shortcomings in the development of photothermal materials: (i) the photothermal mechanism is still unclear, and the role of ultraviolet light in photothermal catalysis is not clear. Photothermal materials should focus on the effect of the coupling between the photothermal effect and the catalytic reaction interface on the photothermal performance; (ii) the test of catalyst surface temperature is not allowed, and the influence mechanism of temperature gradient on photothermal catalytic activity and selectivity at the nanometer scale needs to be studied in

depth; (iii) the comparative advantages and application scenarios of photothermal seawater evaporation and photothermal catalysis as compared with traditional water treatment technology and thermochemical industry have yet to be verified; (iv) the measurement standard of photothermal catalytic activity has not been unified; (v) the theoretical simulations on the photothermal effect during interfacial physicochemical processes are still lacking. Given this, developing photothermal materials for environmental and catalytic applications remains ongoing and a lot of research work is still needed.

Author Contributions: Conceptualization, H.C. and R.S.; writing—original draft preparation, H.C.; writing—review and editing, R.S. and T.Z. All authors have read and agreed to the published version of the manuscript.

References

1. Jiang, X.; Nie, X.; Guo, X.; Song, C.; Chen, J.G. Recent advances in carbon dioxide hydrogenation to methanol via heterogeneous catalysis. *Chem. Rev.* **2020**, *120*, 7984–8034. [CrossRef] [PubMed]
2. Kho, E.T.; Tan, T.H.; Lovell, E.; Wong, R.J.; Scott, J.; Amal, R. A review on photo-thermal catalytic conversion of carbon dioxide. *Green Energy Environ.* **2017**, *2*, 204–217. [CrossRef]
3. Munday, P.L.; Dixson, D.L.; Welch, M.J.; Chivers, D.P.; Domenici, P.; Grosell, M.; Heuer, R.M.; Jones, G.P.; McCormick, M.I.; Meekan, M.; et al. Methods matter in repeating ocean acidification studies. *Nature* **2020**, *586*, E20–E24. [CrossRef]
4. Mekhilef, S.; Saidur, R.; Safari, A. A review on solar energy use in industries. *Renew. Sust. Energy Rev.* **2011**, *15*, 1777–1790. [CrossRef]
5. Alami, A.H.; Aokal, K. Enhancement of spectral absorption of solar thermal collectors by bulk graphene addition via high-pressure graphite blasting. *Energy Convers. Manag.* **2018**, *156*, 757–764. [CrossRef]
6. Campos, C.; Vasco, D.; Angulo, C.; Burdiles, P.A.; Cardemil, J.; Palza, H. About the relevance of particle shape and graphene oxide on the behavior of direct absorption solar collectors using metal based nanofluids under different radiation intensities. *Energy Convers. Manag.* **2019**, *181*, 247–257. [CrossRef]
7. Chandrashekara, M.; Yadav, A. Water desalination system using solar heat: A review. *Renew. Sust. Energy Rev.* **2017**, *67*, 1308–1330. [CrossRef]
8. Shan, X.; Zhao, A.; Lin, Y.; Hu, Y.; Di, Y.; Liu, C.; Gan, Z. Low-cost, scalable, and reusable photothermal layers for highly efficient solar steam generation and versatile energy Conversion. *Adv. Sustain. Syst.* **2020**, *4*, 1900153. [CrossRef]
9. Li, Z.; Liu, J.; Shi, R.; Waterhouse, G.I.N.; Wen, X.D.; Zhang, T. Fe-based catalysts for the direct photohydrogenation of CO_2 to value-added hydrocarbons. *Adv. Energy Mater.* **2021**, *11*, 2002783. [CrossRef]
10. Luo, S.; Ren, X.; Lin, H.; Song, H.; Ye, J. Plasmonic photothermal catalysis for solar-to-fuel conversion: Current status and prospects. *Chem. Sci.* **2021**, *12*, 5701–5719. [CrossRef]
11. Du, J.; Du, Z.; Hu, J.-S.; Pan, Z.; Shen, Q.; Sung, J.; Long, D.; Dong, H.; Sun, L.; Zhong, X.; et al. Zn-Cu-In-Se quantum dot solar cells with a certified power conversion efficiency of 11.6%. *J. Am. Chem. Soc.* **2016**, *138*, 4201–4209. [CrossRef]
12. Giordano, F.; Abate, A.; Baena, J.P.C.; Saliba, M.; Matsui, T.; Im, S.H.; Zakeeruddin, S.M.; Nazeeruddin, M.K.; Hagfeldt, A.; Graetzel, M. Enhanced electronic properties in mesoporous TiO_2 via lithium doping for high-efficiency perovskite solar cells. *Nat. Commun.* **2016**, *7*, 10379. [CrossRef]
13. Jiang, C.; Moniz, S.J.A.; Wang, A.; Zhang, T.; Tang, J. Photoelectrochemical devices for solar water splitting-materials and challenges. *Chem. Soc. Rev.* **2017**, *46*, 4645–4660. [CrossRef] [PubMed]
14. Tan, C.; Cao, X.; Wu, X.-J.; He, Q.; Yang, J.; Zhang, X.; Chen, J.; Zhao, W.; Han, S.; Nam, G.-H.; et al. Recent advances in ultrathin two-dimensional nanomaterials. *Chem. Rev.* **2017**, *117*, 6225–6331. [CrossRef]
15. Wang, P.; Guo, S.; Wang, H.J.; Chen, K.K.; Zhang, N.; Zhang, Z.M.; Lu, T.B. A broadband and strong visible-light-absorbing photosensitizer boosts hydrogen evolution. *Nat. Commun.* **2019**, *10*, 3155. [CrossRef]
16. Wang, Z.; Li, C.; Domen, K. Recent developments in heterogeneous photocatalysts for solar-driven overall water splitting. *Chem. Soc. Rev.* **2019**, *48*, 2109–2125. [CrossRef]
17. Xiong, X.; Mao, C.; Yang, Z.; Zhang, Q.; Waterhouse, G.I.N.; Gu, L.; Zhang, T. Photocatalytic CO_2 reduction to CO over Ni single atoms supported on defect-rich zirconia. *Adv. Energy Mater.* **2020**, *10*, 2002928. [CrossRef]

18. Zhao, Y.; Chen, G.; Bian, T.; Zhou, C.; Waterhouse, G.I.N.; Wu, L.-Z.; Tung, C.-H.; Smith, L.J.; O'Hare, D.; Zhang, T. Defect-rich ultrathin ZnAl-layered double hydroxide nanosheets for efficient photoreduction of CO_2 to CO with water. *Adv. Mater.* **2015**, *27*, 7824–7831. [CrossRef]

19. Zhang, S.; Zhao, Y.; Shi, R.; Zhou, C.; Waterhouse, G.I.N.; Wang, Z.; Weng, Y.; Zhang, T. Sub-3 nm ultrafine Cu_2O for visible light driven nitrogen fixation. *Angew. Chem. Int. Ed.* **2021**, *60*, 2554–2560. [CrossRef] [PubMed]

20. Wu, X.; Chen, G.Y.; Owens, G.; Chu, D.; Xu, H. Photothermal materials: A key platform enabling highly efficient water evaporation driven by solar energy. *Mater. Today Energy* **2019**, *12*, 277–296. [CrossRef]

21. Ghoussoub, M.; Xia, M.; Duchesne, P.N.; Segal, D.; Ozin, G. Principles of photothermal gas-phase heterogeneous CO_2 catalysis. *Energy Environ. Sci.* **2019**, *12*, 1122–1142. [CrossRef]

22. Li, Y.; Li, R.; Li, Z.; Wei, W.; Ouyang, S.; Yuan, H.; Zhang, T. Effect of support on catalytic performance of photothermal Fischer-Tropsch synthesis to produce lower olefins over Fe_5C_2-based catalysts. *Chem. Res. Chin. Univ.* **2020**, *36*, 1006–1012. [CrossRef]

23. Marxer, D.; Furler, P.; Takacs, M.; Steinfeld, A. Solar thermochemical splitting of CO_2 into separate streams of CO and O_2 with high selectivity, stability, conversion, and efficiency. *Energy Environ. Sci.* **2017**, *10*, 1142–1149. [CrossRef]

24. Mateo, D.; Cerrillo, J.L.; Durini, S.; Gascon, J. Fundamentals and applications of photo-thermal catalysis. *Chem. Soc. Rev.* **2021**, *50*, 2173–2210. [CrossRef]

25. Fan, W.K.; Tahir, M. Recent developments in photothermal reactors with understanding on the role of light/heat for CO_2 hydrogenation to fuels: A review. *Chem. Eng. J.* **2022**, *427*, 131617. [CrossRef]

26. Liu, H.; Shi, L.; Zhang, Q.; Qi, P.; Zhao, Y.; Meng, Q.; Feng, X.; Wang, H.; Ye, J. Photothermal catalysts for hydrogenation reactions. *Chem. Commun.* **2021**, *57*, 1279–1294. [CrossRef] [PubMed]

27. Guo, J.; Duchesne, P.N.; Wang, L.; Song, R.; Xia, M.; Ulmer, U.; Sun, W.; Dong, Y.; Loh, J.Y.Y.; Kherani, N.P.; et al. High-performance, scalable, and low-cost copper hydroxyapatite for photothermal CO_2 reduction. *ACS Catal.* **2020**, *10*, 13668–13681. [CrossRef]

28. Zhang, F.; Li, Y.-H.; Qi, M.-Y.; Yamada, Y.M.A.; Anpo, M.; Tang, Z.-R.; Xu, Y.-J. Photothermal catalytic CO_2 reduction over nanomaterials. *Chem Catal.* **2021**, *1*, 272–297. [CrossRef]

29. Ibrahim, I.; Seo, D.H.; McDonagh, A.M.; Shon, H.K.; Tijing, L. Semiconductor photothermal materials enabling efficient solar steam generation toward desalination and wastewater treatment. *Desalination* **2021**, *500*, 114853. [CrossRef]

30. Zhu, L.; Gao, M.; Peh, C.K.N.; Ho, G.W. Solar-driven photothermal nanostructured materials designs and prerequisites for evaporation and catalysis applications. *Mater. Horiz.* **2018**, *5*, 323–343. [CrossRef]

31. Lewis, N.S. Research opportunities to advance solar energy utilization. *Science* **2016**, *351*, aad1920. [CrossRef] [PubMed]

32. Vinoth Kanna, I.; Pinky, D. Solar research—A review and recommendations for the most important supplier of energy for the earth with solar systems. *Int. J. Ambient Energy* **2018**, *41*, 962–968. [CrossRef]

33. Crabtree, G.W.; Lewis, N.S. Solar energy conversion. *Phys. Today* **2007**, *60*, 37–42. [CrossRef]

34. Panwar, N.L.; Kaushik, S.C.; Kothari, S. Role of renewable energy sources in environmental protection: A review. *Renew. Sust. Energy Rev.* **2011**, *15*, 1513–1524. [CrossRef]

35. Habisreutinger, S.N.; Schmidt-Mende, L.; Stolarczyk, J.K. Photocatalytic reduction of CO_2 on TiO_2 and other semiconductors. *Angew. Chem. Int. Ed.* **2013**, *52*, 7372–7408. [CrossRef] [PubMed]

36. Ansari, M.I.H.; Qurashi, A.; Nazeeruddin, M.K. Frontiers, opportunities, and challenges in perovskite solar cells: A critical review. *J. Photochem. Photobiol. C* **2018**, *35*, 1–24. [CrossRef]

37. Hou, W.; Xiao, Y.; Han, G.; Lin, J.Y. The applications of polymers in solar cells: A review. *Polymers* **2019**, *11*, 143. [CrossRef]

38. Yu, Z.; Liu, H.; Zhu, M.; Li, Y.; Li, W. Interfacial charge transport in 1D TiO_2 based photoelectrodes for photoelectrochemical water splitting. *Small* **2021**, *17*, 1903378. [CrossRef]

39. Zarei, E.; Ojani, R. Fundamentals and some applications of photoelectrocatalysis and effective factors on its efficiency: A review. *J. Solid State Electrochem.* **2016**, *21*, 305–336. [CrossRef]

40. Wang, J.; Wei, Y.; Yang, B.; Wang, B.; Chen, J.; Jing, H. In situ grown heterojunction of Bi_2WO_6/BiOCl for efficient photoelectrocatalytic CO_2 reduction. *J. Catal.* **2019**, *377*, 209–217. [CrossRef]

41. Zhao, G.; Huang, X.; Wang, X.; Wang, X. Progress in catalyst exploration for heterogeneous CO_2 reduction and utilization: A critical review. *J. Mater. Chem. A* **2017**, *5*, 21625–21649. [CrossRef]

42. Wang, H.; Xia, Y.; Li, H.; Wang, X.; Yu, Y.; Jiao, X.; Chen, D. Highly active deficient ternary sulfide photoanode for photoelectrochemical water splitting. *Nat. Commun.* **2020**, *11*, 3078. [CrossRef] [PubMed]

43. Fujishima, A.; Honda, K. Electrochemical photolysis of water at a semiconductor electrode. *Nature* **1972**, *238*, 37–38. [CrossRef]

44. Maeda, K.; Domen, K. Photocatalytic water splitting: Recent progress and future challenges. *J. Phys. Chem. Lett.* **2010**, *1*, 2655–2661. [CrossRef]

45. Yuan, L.; Qi, M.Y.; Tang, Z.R.; Xu, Y.J. Coupling strategy for CO_2 valorization integrated with organic synthesis by heterogeneous photocatalysis. *Angew. Chem. Int. Ed.* **2021**, *60*, 21150–21172. [CrossRef]

46. Zhang, W.; Mohamed, A.R.; Ong, W.J. Z-Scheme photocatalytic systems for carbon dioxide reduction: Where are we now? *Angew. Chem. Int. Ed.* **2020**, *59*, 22894–22915. [CrossRef] [PubMed]

47. Shi, R.; Zhang, X.; Waterhouse, G.I.N.; Zhao, Y.; Zhang, T. The journey toward low temperature, low pressure catalytic nitrogen fixation. *Adv. Energy Mater.* **2020**, *10*, 2000659. [CrossRef]

48. Lin, Y.; Xu, H.; Shan, X.; Di, Y.; Zhao, A.; Hu, Y.; Gan, Z. Solar steam generation based on the photothermal effect: From designs to applications, and beyond. *J. Mater. Chem. A* **2019**, *7*, 19203–19227. [CrossRef]

49. Lu, Q.; Yang, Y.; Feng, J.; Wang, X. Oxygen-defected molybdenum oxides hierarchical nanostructure constructed by atomic-level thickness nanosheets as an efficient absorber for solar steam generation. *Sol. RRL* **2019**, *3*, 1800277. [CrossRef]

50. Xie, Z.; Duo, Y.; Lin, Z.; Fan, T.; Xing, C.; Yu, L.; Wang, R.; Qiu, M.; Zhang, Y.; Zhao, Y.; et al. The rise of 2D photothermal materials beyond graphene for clean water production. *Adv. Sci.* **2020**, *7*, 1902236. [CrossRef]

51. Zha, X.J.; Zhao, X.; Pu, J.H.; Tang, L.S.; Ke, K.; Bao, R.Y.; Bai, L.; Liu, Z.Y.; Yang, M.B.; Yang, W. Flexible anti-biofouling MXene/cellulose fibrous membrane for sustainable solar-driven water purification. *ACS Appl. Mater. Interfaces* **2019**, *11*, 36589–36597. [CrossRef] [PubMed]

52. Li, Z.; Liu, J.; Zhao, Y.; Shi, R.; Waterhouse, G.I.N.; Wang, Y.; Wu, L.-Z.; Tung, C.-H.; Zhang, T. Photothermal hydrocarbon synthesis using alumina-supported cobalt metal nanoparticle catalysts derived from layered-double-hydroxide nanosheets. *Nano Energy* **2019**, *60*, 467–475. [CrossRef]

53. Ni, W.; Kou, X.; Yang, Z.; Wang, J. Tailoring longitudinal surface plasmon wavelengths, scattering and absorption cross sections of gold nanorods. *ACS Nano* **2008**, *2*, 677–686. [CrossRef] [PubMed]

54. Boerigter, C.; Campana, R.; Morabito, M.; Linic, S. Evidence and implications of direct charge excitation as the dominant mechanism in plasmon-mediated photocatalysis. *Nat. Commun.* **2016**, *7*, 10545. [CrossRef] [PubMed]

55. Huang, X.; Tang, S.; Mu, X.; Dai, Y.; Chen, G.; Zhou, Z.; Ruan, F.; Yang, Z.; Zheng, N. Freestanding palladium nanosheets with plasmonic and catalytic properties. *Nat. Nanotechnol.* **2011**, *6*, 28–32. [CrossRef]

56. Wang, F.; Li, C.; Chen, H.; Jiang, R.; Sun, L.D.; Li, Q.; Wang, J.; Yu, J.C.; Yan, C.H. Plasmonic harvesting of light energy for Suzuki coupling reactions. *J. Am. Chem. Soc.* **2013**, *135*, 5588–5601. [CrossRef]

57. Chen, G.; Gao, R.; Zhao, Y.; Li, Z.; Waterhouse, G.I.N.; Shi, R.; Zhao, J.; Zhang, M.; Shang, L.; Sheng, G.; et al. Alumina-supported CoFe alloy catalysts derived from layered-double-hydroxide nanosheets for efficient photothermal CO$_2$ hydrogenation to hydrocarbons. *Adv. Mater.* **2018**, *30*, 1704663. [CrossRef]

58. Huang, H.; Mao, M.; Zhang, Q.; Li, Y.; Bai, J.; Yang, Y.; Zeng, M.; Zhao, X. Solar-light-driven CO$_2$ reduction by CH$_4$ on silica-cluster-modified Ni nanocrystals with a high solar-to-fuel efficiency and excellent durability. *Adv. Energy Mater.* **2018**, *8*, 1702472. [CrossRef]

59. Tong, Z.; Yang, D.; Shi, J.; Nan, Y.; Sun, Y.; Jiang, Z. Three-dimensional porous aerogel constructed by g-C$_3$N$_4$ and graphene oxide nanosheets with excellent visible-light photocatalytic performance. *ACS Appl. Mater. Interfaces* **2015**, *7*, 25693–25701. [CrossRef]

60. Zhou, S.; Shang, L.; Zhao, Y.; Shi, R.; Waterhouse, G.I.N.; Huang, Y.C.; Zheng, L.; Zhang, T. Pd single-atom catalysts on nitrogen-doped graphene for the highly selective photothermal hydrogenation of acetylene to ethylene. *Adv. Mater.* **2019**, *31*, 1900509. [CrossRef]

61. Han, C.; Li, J.; Ma, Z.; Xie, H.; Waterhouse, G.I.N.; Ye, L.; Zhang, T. Black phosphorus quantum dot/g-C$_3$N$_4$ composites for enhanced CO$_2$ photoreduction to CO. *Sci. China Mater.* **2018**, *61*, 1159–1166. [CrossRef]

62. Liu, G.; Meng, X.; Zhang, H.; Zhao, G.; Pang, H.; Wang, T.; Li, P.; Kako, T.; Ye, J. Elemental boron for efficient carbon dioxide reduction under light irradiation. *Angew. Chem. Int. Ed.* **2017**, *56*, 5570–5574. [CrossRef] [PubMed]

63. Hoch, L.B.; O'Brien, P.G.; Jelle, A.; Sandhel, A.; Perovic, D.D.; Mims, C.A.; Ozin, G.A. Nanostructured indium oxide coated silicon nanowire arrays: A hybrid photothermal/photochemical approach to solar fuels. *ACS Nano* **2016**, *10*, 9017–9025. [CrossRef]

64. Wu, D.; Deng, K.; Hu, B.; Lu, Q.; Liu, G.; Hong, X. Plasmon-assisted photothermal catalysis of low-pressure CO$_2$ hydrogenation to methanol over Pd/ZnO Catalyst. *ChemCatChem* **2019**, *11*, 1598–1601. [CrossRef]

65. Deng, Z.; Zhou, J.; Miao, L.; Liu, C.; Peng, Y.; Sun, L.; Tanemura, S. The emergence of solar thermal utilization: Solar-driven steam generation. *J. Mater. Chem. A* **2017**, *5*, 7691–7709. [CrossRef]

66. Lalisse, A.; Tessier, G.; Plain, J.; Baffou, G. Quantifying the efficiency of plasmonic materials for near-field enhancement and photothermal conversion. *J. Phys. Chem. C* **2015**, *119*, 25518–25528. [CrossRef]

67. Song, H.; Meng, X.; Dao, T.D.; Zhou, W.; Liu, H.; Shi, L.; Zhang, H.; Nagao, T.; Kako, T.; Ye, J. Light-enhanced carbon dioxide activation and conversion by effective plasmonic coupling effect of Pt and Au nanoparticles. *ACS Appl. Mater. Interfaces* **2018**, *10*, 408–416. [CrossRef]

68. Gao, P.; Li, S.; Bu, X.; Dang, S.; Liu, Z.; Wang, H.; Zhong, L.; Qiu, M.; Yang, C.; Cai, J.; et al. Direct conversion of CO$_2$ into liquid fuels with high selectivity over a bifunctional catalyst. *Nat. Chem.* **2017**, *9*, 1019–1024. [CrossRef]

69. Rodemerck, U.; Holeňa, M.; Wagner, E.; Smejkal, Q.; Barkschat, A.; Baerns, M. Catalyst development for CO$_2$ hydrogenation to fuels. *ChemCatChem* **2013**, *5*, 1948–1955. [CrossRef]

70. Wei, J.; Ge, Q.; Yao, R.; Wen, Z.; Fang, C.; Guo, L.; Xu, H.; Sun, J. Directly converting CO$_2$ into a gasoline fuel. *Nat. Commun.* **2017**, *8*, 15174. [CrossRef]

71. Liu, Y.; de Tymowski, B.; Vigneron, F.; Florea, I.; Ersen, O.; Meny, C.; Nguyen, P.; Pham, C.; Luck, F.; Pham-Huu, C. Titania-decorated silicon carbide-containing cobalt catalyst for Fischer–Tropsch synthesis. *ACS Catal.* **2013**, *3*, 393–404. [CrossRef]

72. Zhong, L.; Yu, F.; An, Y.; Zhao, Y.; Sun, Y.; Li, Z.; Lin, T.; Lin, Y.; Qi, X.; Dai, Y.; et al. Cobalt carbide nanoprisms for direct production of lower olefins from syngas. *Nature* **2016**, *538*, 84–87. [CrossRef]

73. Xu, M.; Hu, X.; Wang, S.; Yu, J.; Zhu, D.; Wang, J. Photothermal effect promoting CO$_2$ conversion over composite photocatalyst with high graphene content. *J. Catal.* **2019**, *377*, 652–661. [CrossRef]

74. Wang, S.; Shang, L.; Li, L.; Yu, Y.; Chi, C.; Wang, K.; Zhang, J.; Shi, R.; Shen, H.; Waterhouse, G.I.; et al. Metal-organic-framework-derived mesoporous carbon nanospheres containing porphyrin-like metal centers for conformal phototherapy. *Adv. Mater.* **2016**, *28*, 8379–8387. [CrossRef] [PubMed]

75. Wang, X.; He, Y.; Cheng, G.; Shi, L.; Liu, X.; Zhu, J. Direct vapor generation through localized solar heating via carbon-nanotube nanofluid. *Energy Convers. Manag.* **2016**, *130*, 176–183. [CrossRef]

76. Gan, Z.; Wu, X.; Meng, M.; Zhu, X.; Yang, L.; Chu, P.K. Photothermal contribution to enhanced photocatalytic performance of graphene-based nanocomposites. *ACS Nano* **2014**, *8*, 9304–9310. [CrossRef]

77. Song, J.; Wang, F.; Yang, X.; Ning, B.; Harp, M.G.; Culp, S.H.; Hu, S.; Huang, P.; Nie, L.; Chen, J.; et al. Gold nanoparticle coated carbon nanotube ring with enhanced raman scattering and photothermal conversion property for theranostic applications. *J. Am. Chem. Soc.* **2016**, *138*, 7005–7015. [CrossRef] [PubMed]

78. O'Brien, P.G.; Sandhel, A.; Wood, T.E.; Jelle, A.A.; Hoch, L.B.; Perovic, D.D.; Mims, C.A.; Ozin, G.A. Photomethanation of gaseous CO_2 over Ru/silicon nanowire catalysts with visible and near-infrared photons. *Adv. Sci.* **2014**, *1*, 1400001. [CrossRef]

79. Zhao, H.; Chen, H.; Guo, Z.; Zhang, W.; Yu, H.; Zhuang, Z.; Zhong, H.; Liu, Z. In situ photothermal activation of necroptosis potentiates black phosphorus-mediated cancer photo-immunotherapy. *Chem. Eng. J.* **2020**, *394*, 124314. [CrossRef]

80. Gude, V.G. Desalination and sustainability—An appraisal and current perspective. *Water Res.* **2016**, *89*, 87–106. [CrossRef]

81. Shao, B.; Wang, Y.; Wu, X.; Lu, Y.; Yang, X.; Chen, G.Y.; Owens, G.; Xu, H. Stackable nickel–cobalt@polydopamine nanosheet based photothermal sponges for highly efficient solar steam generation. *J. Mater. Chem. A* **2020**, *8*, 11665–11673. [CrossRef]

82. Li, R.; Zhang, L.; Shi, L.; Wang, P. MXene Ti_3C_2: An effective 2D light-to-heat conversion material. *ACS Nano* **2017**, *11*, 3752–3759. [CrossRef] [PubMed]

83. Ghim, D.; Jiang, Q.; Cao, S.; Singamaneni, S.; Jun, Y.-S. Mechanically interlocked 1T/2H phases of MoS_2 nanosheets for solar thermal water purification. *Nano Energy* **2018**, *53*, 949–957. [CrossRef]

84. Yao, J.; Yang, G. An efficient solar-enabled 2D layered alloy material evaporator for seawater desalination. *J. Mater. Chem. A* **2018**, *6*, 3869–3876. [CrossRef]

85. Yang, X.; Yang, Y.; Fu, L.; Zou, M.; Li, Z.; Cao, A.; Yuan, Q. An ultrathin flexible 2D membrane based on single-walled nanotube-MoS_2 hybrid film for high-performance solar steam generation. *Adv. Funct. Mater.* **2018**, *28*, 1704505. [CrossRef]

86. Li, K.; Chang, T.H.; Li, Z.; Yang, H.; Fu, F.; Li, T.; Ho, J.S.; Chen, P.Y. Biomimetic MXene textures with enhanced light-to-heat conversion for solar steam generation and wearable thermal management. *Adv. Energy Mater.* **2019**, *9*, 1901687. [CrossRef]

87. Ming, X.; Guo, A.; Wang, G.; Wang, X. Two-dimensional defective tungsten oxide nanosheets as high performance photo-absorbers for efficient solar steam generation. *Sol. Energy Mater. Sol. Cells* **2018**, *185*, 333–341. [CrossRef]

88. Yin, J.; You, X.; Zhang, Z.; Guo, Z.; Wang, J.; Wang, X. Boron nanosheets loaded with MoS_2 porous sponges for water purification. *J. Water Process. Eng.* **2021**, *41*, 102048. [CrossRef]

89. Yang, Y.; Yang, X.; Fu, L.; Zou, M.; Cao, A.; Du, Y.; Yuan, Q.; Yan, C.-H. Two-dimensional flexible bilayer janus membrane for advanced photothermal water desalination. *ACS Energy Lett.* **2018**, *3*, 1165–1171. [CrossRef]

90. Qu, W.; Zhao, H.; Zhang, Q.; Xia, D.; Tang, Z.; Chen, Q.; He, C.; Shu, D. Multifunctional Au/Ti_3C_2 photothermal membrane with antibacterial ability for stable and efficient solar water purification under the full spectrum. *ACS Sustain. Chem. Eng.* **2021**, *9*, 11372–11387. [CrossRef]

91. Zhu, L.; Gao, M.; Peh, C.K.N.; Wang, X.; Ho, G.W. Self-contained monolithic carbon sponges for solar-driven interfacial water evaporation distillation and electricity generation. *Adv. Energy Mater.* **2018**, *8*, 1702149. [CrossRef]

92. Liang, H.; Liao, Q.; Chen, N.; Liang, Y.; Lv, G.; Zhang, P.; Lu, B.; Qu, L. Thermal efficiency of solar steam generation approaching 100% through capillary water transport. *Angew. Chem. Int. Ed.* **2019**, *58*, 19041–19046. [CrossRef]

93. Fu, Y.; Wang, G.; Ming, X.; Liu, X.; Hou, B.; Mei, T.; Li, J.; Wang, J.; Wang, X. Oxygen plasma treated graphene aerogel as a solar absorber for rapid and efficient solar steam generation. *Carbon* **2018**, *130*, 250–256. [CrossRef]

94. Zhang, Z.; Mu, P.; He, J.; Zhu, Z.; Sun, H.; Wei, H.; Liang, W.; Li, A. Facile and scalable fabrication of surface-modified sponge for efficient solar steam generation. *ChemSusChem* **2019**, *12*, 426–433. [CrossRef]

95. Hu, X.; Xu, W.; Zhou, L.; Tan, Y.; Wang, Y.; Zhu, S.; Zhu, J. Tailoring graphene oxide-based aerogels for efficient solar steam generation under one sun. *Adv. Mater.* **2017**, *29*, 160431. [CrossRef] [PubMed]

96. Mu, P.; Zhang, Z.; Bai, W.; He, J.; Sun, H.; Zhu, Z.; Liang, W.; Li, A. Superwetting monolithic hollow-carbon-nanotubes aerogels with hierarchically nanoporous structure for efficient solar steam generation. *Adv. Energy Mater.* **2019**, *9*, 1802158. [CrossRef]

97. Fan, X.; Yang, Y.; Shi, X.; Liu, Y.; Li, H.; Liang, J.; Chen, Y. A MXene-based hierarchical design enabling highly efficient and stable solar-water desalination with good salt resistance. *Adv. Funct. Mater.* **2020**, *30*, 2007110. [CrossRef]

98. Wang, Z.; Yu, K.; Gong, S.; Mao, H.; Huang, R.; Zhu, Z. Cu_3BiS_3/MXenes with excellent solar-thermal conversion for continuous and efficient seawater desalination. *ACS Appl. Mater. Interfaces* **2021**, *13*, 16246–16258. [CrossRef]

99. Zhang, J.; Luo, X.; Zhang, X.; Xu, Y.; Xu, H.; Zuo, J.; Liu, D.; Cui, F.; Wang, W. Three-dimensional porous photo-thermal fiber felt with salt-resistant property for high efficient solar distillation. *Chin. Chem. Lett.* **2021**, *32*, 1442–1446. [CrossRef]

100. Yuan, J.; Lei, X.; Yi, C.; Jiang, H.; Liu, F.; Cheng, G.J. 3D-printed hierarchical porous cellulose/alginate/carbon black hydrogel for high-efficiency solar steam generation. *Chem. Eng. J.* **2022**, *430*, 132765. [CrossRef]

101. Storer, D.P.; Phelps, J.L.; Wu, X.; Owens, G.; Khan, N.I.; Xu, H. Graphene and rice-straw-fiber-based 3D photothermal aerogels for highly efficient solar evaporation. *ACS Appl. Mater. Interfaces* **2020**, *12*, 15279–15287. [CrossRef]

102. Novoselov, K.S.; Geim, A.K.; Morozov, S.V.; Jiang, D.; Zhang, Y.; Dubonos, S.V.; Grigorieva, I.V.; Firsov, A.A. Electric field effect in atomically thin carbon films. *Science* **2004**, *306*, 666–669. [CrossRef] [PubMed]

103. Liu, G.; Jin, W.; Xu, N. Two-dimensional-material membranes: A new family of high-performance separation membranes. *Angew. Chem. Int. Ed.* **2016**, *55*, 13384–13397. [CrossRef]

104. Alhabeb, M.; Maleski, K.; Anasori, B.; Lelyukh, P.; Clark, L.; Sin, S.; Gogotsi, Y. Guidelines for synthesis and processing of two-dimensional titanium carbide ($Ti_3C_2T_x$ MXene). *Chem. Mater.* **2017**, *29*, 7633–7644. [CrossRef]

105. Xu, D.; Li, Z.; Li, L.; Wang, J. Insights into the photothermal conversion of 2D MXene nanomaterials: Synthesis, mechanism, and applications. *Adv. Funct. Mater.* **2020**, *30*, 2000712. [CrossRef]

106. Wang, Z.; Xu, W.; Yu, K.; Gong, S.; Mao, H.; Huang, R.; Zhu, Z. NiS_2 nanocubes coated Ti_3C_2 nanosheets with enhanced light-to-heat conversion for fast and efficient solar seawater steam generation. *Sol. RRL* **2021**, *5*, 2100183. [CrossRef]

107. Xie, Z.; Peng, Y.-P.; Yu, L.; Xing, C.; Qiu, M.; Hu, J.; Zhang, H. Solar-inspired water purification based on emerging 2D materials: Status and challenges. *Sol. RRL* **2020**, *4*, 1900400. [CrossRef]

108. Gu, Y.; Jiao, Y.; Zhou, X.; Wu, A.; Buhe, B.; Fu, H. Strongly coupled Ag/TiO_2 heterojunctions for effective and stable photothermal catalytic reduction of 4-nitrophenol. *Nano Res.* **2018**, *11*, 126–141. [CrossRef]

109. Nikitenko, S.I.; Chave, T.; Cau, C.; Brau, H.-P.; Flaud, V. Photothermal hydrogen production using noble-metal-free $Ti@TiO_2$ core–shell nanoparticles under visible–NIR light irradiation. *ACS Catal.* **2015**, *5*, 4790–4795. [CrossRef]

110. Song, R.; Luo, B.; Geng, J.; Song, D.; Jing, D. Photothermocatalytic hydrogen evolution over Ni_2P/TiO_2 for full-spectrum solar energy conversion. *Ind. Eng. Chem. Res.* **2018**, *57*, 7846–7854. [CrossRef]

111. Wang, Z.J.; Song, H.; Liu, H.; Ye, J. Coupling of solar energy and thermal energy for carbon dioxide reduction: Status and prospects. *Angew. Chem. Int. Ed.* **2020**, *59*, 8016–8035. [CrossRef] [PubMed]

112. Jia, J.; Wang, H.; Lu, Z.; O'Brien, P.G.; Ghoussoub, M.; Duchesne, P.; Zheng, Z.; Li, P.; Qiao, Q.; Wang, L.; et al. Photothermal catalyst engineering: Hydrogenation of gaseous CO_2 with high activity and tailored selectivity. *Adv. Sci.* **2017**, *4*, 1700252. [CrossRef] [PubMed]

113. Wang, L.; Wang, Y.; Cheng, Y.; Liu, Z.; Guo, Q.; Ha, M.N.; Zhao, Z. Hydrogen-treated mesoporous WO_3 as a reducing agent of CO_2 to fuels (CH_4 and CH_3OH) with enhanced photothermal catalytic performance. *J. Mater. Chem. A* **2016**, *4*, 5314–5322. [CrossRef]

114. Wang, L.; Ghoussoub, M.; Wang, H.; Shao, Y.; Sun, W.; Tountas, A.A.; Wood, T.E.; Li, H.; Loh, J.Y.Y.; Dong, Y.; et al. Photocatalytic hydrogenation of carbon dioxide with high selectivity to methanol at atmospheric pressure. *Joule* **2018**, *2*, 1369–1381. [CrossRef]

115. Wang, Z.-J.; Song, H.; Pang, H.; Ning, Y.; Dao, T.D.; Wang, Z.; Chen, H.; Weng, Y.; Fu, Q.; Nagao, T.; et al. Photo-assisted methanol synthesis via CO_2 reduction under ambient pressure over plasmonic Cu/ZnO catalysts. *Appl. Catal. B* **2019**, *250*, 10–16. [CrossRef]

116. Liu, L.; Puga, A.V.; Cored, J.; Concepción, P.; Pérez-Dieste, V.; García, H.; Corma, A. Sunlight-assisted hydrogenation of CO_2 into ethanol and C_{2+} hydrocarbons by sodium-promoted Co@C nanocomposites. *Appl. Catal. B* **2018**, *235*, 186–196. [CrossRef]

117. Zhang, W.; Wang, L.; Wang, K.; Khan, M.U.; Wang, M.; Li, H.; Zeng, J. Integration of photothermal effect and heat insulation to efficiently reduce reaction temperature of CO_2 hydrogenation. *Small* **2017**, *13*, 1602583. [CrossRef]

118. Han, B.; Wei, W.; Chang, L.; Cheng, P.; Hu, Y.H. Efficient visible light photocatalytic CO_2 reforming of CH_4. *ACS Catal.* **2016**, *6*, 494–497. [CrossRef]

119. Liu, H.; Meng, X.; Dao, T.D.; Zhang, H.; Li, P.; Chang, K.; Wang, T.; Li, M.; Nagao, T.; Ye, J. Conversion of carbon dioxide by methane reforming under visible-light irradiation: Surface-plasmon-mediated nonpolar molecule activation. *Angew. Chem. Int. Ed.* **2015**, *54*, 11545–11549. [CrossRef]

120. Zhao, Y.; Zhao, B.; Liu, J.; Chen, G.; Gao, R.; Yao, S.; Li, M.; Zhang, Q.; Gu, L.; Xie, J.; et al. Oxide-modified nickel photocatalysts for the production of hydrocarbons in visible light. *Angew. Chem. Int. Ed.* **2016**, *55*, 4215–4219. [CrossRef]

121. Li, Z.; Liu, J.; Zhao, Y.; Waterhouse, G.I.N.; Chen, G.; Shi, R.; Zhang, X.; Liu, X.; Wei, Y.; Wen, X.-D.; et al. Co-based catalysts derived from layered-double-hydroxide nanosheets for the photothermal production of light olefins. *Adv. Mater.* **2018**, *30*, 1800527. [CrossRef] [PubMed]

122. Zhao, Y.; Li, Z.; Li, M.; Liu, J.; Liu, X.; Waterhouse, G.I.N.; Wang, Y.; Zhao, J.; Gao, W.; Zhang, Z.; et al. Reductive transformation of layered-double-hydroxide nanosheets to Fe-based heterostructures for efficient visible-light photocatalytic hydrogenation of CO. *Adv. Mater.* **2018**, *30*, 1803127. [CrossRef] [PubMed]

123. Zhang, Y.; Su, X.; Li, L.; Qi, H.; Yang, C.; Liu, W.; Pan, X.; Liu, X.; Yang, X.; Huang, Y.; et al. Ru/TiO_2 catalysts with size-dependent metal/support interaction for tunable reactivity in Fischer–Tropsch synthesis. *ACS Catal.* **2020**, *10*, 12967–12975. [CrossRef]

124. Sastre, F.; Oteri, M.; Corma, A.; García, H. Photocatalytic water gas shift using visible or simulated solar light for the efficient, room-temperature hydrogen generation. *Energy Environ. Sci.* **2013**, *6*, 2211–2215. [CrossRef]

125. Zhao, L.; Qi, Y.; Song, L.; Ning, S.; Ouyang, S.; Xu, H.; Ye, J. Solar-driven water–gas shift reaction over CuO_x/Al_2O_3 with 1.1 % of light-to-energy storage. *Angew. Chem. Int. Ed.* **2019**, *58*, 7708–7712. [CrossRef]

126. Cavani, F.; Trifirò, F.; Vaccari, A. Hydrotalcite-type anionic clays: Preparation, properties and applications. *Catal. Today* **1991**, *11*, 173–301. [CrossRef]

127. Gursky, J.A.; Blough, S.D.; Luna, C.; Gomez, C.; Luevano, A.N.; Gardner, E.A. Particle-particle interactions between layered double hydroxide nanoparticles. *J. Am. Chem. Soc.* **2006**, *128*, 8376–8377. [CrossRef]

128. Williams, G.R.; O'Hare, D. Towards understanding, control and application of layered double hydroxide chemistry. *J. Mater. Chem.* **2006**, *16*, 3065–3074. [CrossRef]

129. Zhao, Y.; Jia, X.; Waterhouse, G.I.N.; Wu, L.-Z.; Tung, C.-H.; O'Hare, D.; Zhang, T. Layered double hydroxide nanostructured photocatalysts for renewable energy production. *Adv. Energy Mater.* **2016**, *6*, 1501974. [CrossRef]

130. Ren, J.; Ouyang, S.; Xu, H.; Meng, X.; Wang, T.; Wang, D.; Ye, J. Targeting activation of CO_2 and H_2 over Ru-loaded ultrathin layered double hydroxides to achieve efficient photothermal CO_2 methanation in flow-type system. *Adv. Energy Mater.* **2017**, *7*, 1601657. [CrossRef]

131. Li, Z.; Shi, R.; Zhao, J.; Zhang, T. Ni-based catalysts derived from layered-double-hydroxide nanosheets for efficient photothermal CO_2 reduction under flow-type system. *Nano Res.* **2021**, *14*, 4828–4832. [CrossRef]

132. Hoch, L.B.; Wood, T.E.; O'Brien, P.G.; Liao, K.; Reyes, L.M.; Mims, C.A.; Ozin, G.A. The rational design of a single-component photocatalyst for gas-phase CO_2 reduction using both UV and visible Light. *Adv. Sci.* **2014**, *1*, 1400013. [CrossRef]

133. Ghuman, K.K.; Wood, T.E.; Hoch, L.B.; Mims, C.A.; Ozin, G.A.; Singh, C.V. Illuminating CO_2 reduction on frustrated lewis pair surfaces: Investigating the role of surface hydroxides and oxygen vacancies on nanocrystalline $In_2O_{3-x}(OH)_y$. *Phys. Chem. Chem. Phys.* **2015**, *17*, 14623–14635. [CrossRef]

134. Nguyen, N.T.; Xia, M.; Duchesne, P.N.; Wang, L.; Mao, C.; Jelle, A.A.; Yan, T.; Li, P.; Lu, Z.H.; Ozin, G.A. Enhanced CO_2 photocatalysis by indium oxide hydroxide supported on TiN@TiO_2 nanotubes. *Nano Lett.* **2021**, *21*, 1311–1319. [CrossRef]

135. Liu, H.; Song, H.; Zhou, W.; Meng, X.; Ye, J. A promising application of optical hexagonal TaN in photocatalytic reactions. *Angew. Chem. Int. Ed.* **2018**, *57*, 16781–16784. [CrossRef] [PubMed]

136. Liu, H.; Dao, T.D.; Liu, L.; Meng, X.; Nagao, T.; Ye, J. Light assisted CO_2 reduction with methane over group VIII metals: Universality of metal localized surface plasmon resonance in reactant activation. *Appl. Catal. B* **2017**, *209*, 183–189. [CrossRef]

137. Zhang, H.; Wang, T.; Wang, J.; Liu, H.; Dao, T.D.; Li, M.; Liu, G.; Meng, X.; Chang, K.; Shi, L.; et al. Surface-plasmon-enhanced photodriven CO_2 reduction catalyzed by metal–organic-framework-derived iron nanoparticles encapsulated by ultrathin carbon layers. *Adv. Mater.* **2016**, *28*, 3703–3710. [CrossRef] [PubMed]

138. Song, H.; Meng, X.; Wang, Z.-J.; Wang, Z.; Chen, H.; Weng, Y.; Ichihara, F.; Oshikiri, M.; Kako, T.; Ye, J. Visible-light-mediated methane activation for steam methane reforming under mild conditions: A case study of Rh/TiO_2 catalysts. *ACS Catal.* **2018**, *8*, 7556–7565. [CrossRef]